Climate Dynamics (2018) 51:3333–3350
https://doi.org/10.1007/s00382-018-4081-y

Interdecadal variability of the ENSO teleconnection to the wintertime North Pacific

Christopher H. O'Reilly[1]

Received: 3 August 2017 / Accepted: 8 January 2018 / Published online: 8 February 2018

Abstract
The El Niño/Southern Oscillation (ENSO) strongly influences the large-scale atmospheric circulation over the extratropical North Pacific during boreal winter, which has an important impact on North American winter climate. This study analyses the interdecadal variability of the ENSO teleconnection to the wintertime extratropical North Pacific, over the period 1900–2010, using a range of observationally derived datasets and an ensemble of atmospheric model simulations. The observed teleconnection strength is found to vary substantially over the 20th century. Specifically, 31-year periods in the early-century (1912–1942), mid-century (1946–1976) and the late-century (1980–2010) are identified in the observations when the ENSO teleconnection to the North Pacific circulation are found to be particularly strong, weak and strong respectively. The ENSO teleconnection to the North Pacific in the atmospheric model ensemble is weak in the mid-century period and substantially stronger in the late-century, closely following the variability in the observed ENSO-North Pacific teleconnection. In the early-century, however, the atmospheric model also exhibits a weak teleconnection to the North Pacific, unlike in observations. In a subset of the model realisations that exhibit similar ENSO-North Pacific teleconnection as in observations during the early-century period there are large differences in extratropical circulation but not in equatorial Pacific precipitation anomalies, in contrast to the late-century period. This suggests that the high correlation in the early century period is largely due to internal extratropical variability. The important implications of these results for seasonal predictability and the assessment of seasonal forecasting systems are discussed.

Keywords ENSO · Decadal variability · Teleconnections · North Pacific circulation · Seasonal predictability

1 Introduction

The El Niño-Southern Oscillation (ENSO) phenomenon in the equatorial Pacific ocean is one of the most important sources of variability in global climate (McPhaden et al. 2006; Sarachik and Cane 2010). ENSO influences remote regions though "teleconnections" (Bjerknes 1969). The sea surface temperature (SST) anomalies over the eastern equatorial Pacific influence the temperature and precipitation of other regions in the tropics by shifting the location of convection associated with the upward branch of the Walker circulation (e.g. Ropelewski and Halpert 1987). The convection anomalies associated with ENSO also have teleconnections with the extratropics (e.g. Trenberth et al. 1998). The anomalous heating generates anomalous upper-level divergent outflow and associated convergence in the subtropics. This acts as a source of Rossby waves, which propagate into the extratropics and result in large-scale extratropical circulation anomalies that influence seasonal climate (Branstator 1985; Sardeshmukh and Hoskins 1988).

The ENSO teleconnection to the North Pacific is particularly strong during boreal winter, when El Niño events tend to peak. During an El Niño the Aleutian Low tends to deepen and shift south, associated with equivalent barotropic circulation anomalies (Bjerknes 1969; Namias 1976; Horel and Wallace 1981), with approximately opposite anomalies occurring during La Niña events (Trenberth et al. 1998). The wintertime circulation anomalies over the North Pacific are closely related to the Pacific/North American (PNA) pattern

Electronic supplementary material The online version of this article (https://doi.org/10.1007/s00382-018-4081-y) contains supplementary material, which is available to authorized users.

✉ Christopher H. O'Reilly
christopher.oreilly@physics.ox.ac.uk

[1] Atmospheric, Oceanic and Planetary of Physics, University of Oxford, Oxford, UK

(Wallace and Gutzler 1981), and these large-scale circulation anomalies are responsible for significant temperature and precipitation anomalies over North America (e.g. Gershunov and Barnett 1998a; Cayan et al. 1999).

However, previous studies have shown that the observed ENSO teleconnection to the North Pacific exhibits pronounced interdecadal variability, as shown by Gershunov and Barnett (1998b). McCabe and Dettinger (1999) showed that the relationship between ENSO and winter precipitation anomalies over the western United States varies substantially during the 20th century. Minobe and Mantua (1999) found that the relationship between ENSO (measured using both the Southern Oscillation Index and the Cold Tongue Index of equatorial Pacific SSTs) and winter sea-level pressure (SLP) anomalies in the Aleutian Low region was strong in the early and late 20th century but was remarkably weak between 1948–1976. A similar change in correlation was shown by Diaz et al. (2001) in their analysis of the interannual relationship between late winter (February–April) ENSO and 500 hPa geopotential height anomalies over the second half of the 20th century. The shift between weak interannual correlation between ENSO and the Aleutian Low to the stronger correlation after 1977 closely corresponds to the late 1970s climate shift in the Pacific (e.g. Trenberth and Hurrell 1994; Mantua et al. 1997; Minobe 1997; Zhang et al. 1997). After 1977, the amplitude of ENSO events increased (Wang 1995), exerting a stronger forcing on the extratropics (Diaz et al. 2001) and a greater nonlinearity in the response of local surface winds to tropical Pacific SSTs (Wu and Hsieh 2003). However, the shift in interannual correlation during the 1940s—identified by Minobe and Mantua (1999)—does not seem to be associated with such clear changes in ENSO variability (e.g. Trenberth and Shea 1987; Mantua et al. 1997; Deser et al. 2010). Therefore, the characteristics and causes of these apparent interdecadal modulations in the ENSO teleconnection to the wintertime North Pacific circulation remain unclear.

As well as having important implications for Northern extratropical climate variability, the interdecadal variability in the ENSO teleconnection to the North Pacific is also important for seasonal climate predictability. Significant recent developments have resulted in increased skill of seasonal forecast systems for the extratropics in the Northern Hemisphere winter (Scaife et al. 2014; Dunstone et al. 2016). O'Reilly et al. (2017) showed that in Northern Hemisphere seasonal hindcast experiments the skill of the PNA varies dramatically over the 20th century, closely following the observed relationship between ENSO and the PNA. The drop in skill over the North Pacific in the mid-20th century also corresponds to a period of reduced skill in over the Euro-Atlantic sector (Weisheimer et al. 2017; O'Reilly et al. 2017). Understanding the nature of the interdecadal variability in the ENSO teleconnection to the North Pacific is therefore crucial in determining how seasonal forecast skill has varied in the past and may possibly change going forwards.

In this study we investigate the variability of the wintertime ENSO teleconnection to the North Pacific between 1900 and 2010. We analyse modern observational datasets and an ensemble of model simulations. The datasets and simulations are outlined in the following section. We then assess the evidence of interdecadal variability of the ENSO teleconnection to the North Pacific in the observational datasets, in Sect. 3. The ENSO teleconnection variability is then analysed in an ensemble of atmospheric model simulations, in Sect. 4. We finish with a summary and further discussion.

2 Datasets and methods

2.1 Observational datasets

The variability of the ENSO teleconnection is analysed here using a number of observationally derived gridded datasets that are available from 1900 onwards. We restrict our observational analysis to SLP for the North Pacific circulation indices because we are mainly interested in the surface anomalies associated with ENSO. Moreover, extensive upper-air observations are only available during the latter half of the 20th century and only surface observations are assimilated into the 20th century reanalysis products. We employ multiple datasets for both the SST and SLP to give a range of observational uncertainty. Many of these datasets are essentially produced using the same raw observational data and these are associated with their own particular uncertainties, which can be considerable (e.g. Kent et al. 2016). Nonetheless, analysing the various datasets provides a range of observational estimates due to the different data processing techniques, which are expected to be largest where the observations are most uncertain.

We analyse SST anomalies from four gridded monthly products: the NOAA Extended Reconstructed SST v4 (ERSST), provided on a $2° \times 2°$ grid (Huang et al. 2015); the Hadley Centre Sea Ice and SST dataset v2.1 (HadISST), provided on a $1° \times 1°$ grid (Rayner et al. 2003); the Centennial In Situ Observation-Based Estimates of SST v2 (COBE), provided on a $1° \times 1°$ grid (Hirahara et al. 2014); the Kaplan Extended SST v2 (Kaplan), provided on a $5° \times 5°$ grid (Kaplan et al. 1998). Prior to the analysis the climatology from 1900–2010 was removed from each of the datasets individually but no detrending has been applied.

We analyse SLP anomalies from three gridded monthly products. The first is the Hadley Centre SLP dataset v2 (HadSLP), which is produced using surface pressure observations over land and ocean using a statistical interpolation procedure. HadSLP is provided on a $5° \times 5°$ grid (Allan and

Ansell 2006). The second SLP dataset we use is taken from the European Centre for Medium Range Weather Forecasts (ECMWF) 20th century reanalysis (ERA-20C), which is a reanalysis produced by assimilating only surface pressure and marine wind observations (Poli et al. 2016). SLP from ERA-20C was downloaded on a 2.5° × 2.5° grid. The third SLP dataset we use is taken from the NOAA-CIRES 20th century reanalysis v2c (20CR), which was produced by assimilating surface pressure observations using an ensemble filter technique and is available on a 2° × 2° grid (Compo et al. 2006, 2011). In Sect. 4, we also present analysis from the ECMWF ERA-Interim reanalysis product, which is available from 1979 onwards (Dee et al. 2011).

In addition, we analyse cloud-cover anomalies from the ICOADS dataset (Woodruff et al. 2011), which is a proxy for convective precipitation over oceans in the tropics (where precipitation observations are not available prior to the satellite period). This is provided on a 2° × 2° grid. To remove spurious trends due to changes in observational methods we removed the trend of the cloud-cover averaged over the tropics (30°S–30°N) from each grid point, following Deser and Phillips (2006).

Here we analyse data for the boreal winter, defined as the December–January–February average, where the year of each winter refers to the year in which the winter ends (i.e. the DJF winter of 1900/1901 would be referred to as 1901).

2.2 ERA-20CM simulations

In addition to the observational datasets, we also analyse output from ERA-20CM, which is an ensemble of atmospheric model simulations, run between 1899 and 2010 (Hersbach et al. 2015). These simulations consist of 10 freely evolving ensemble members (i.e. they do not assimilate any synoptic atmospheric observations), forced with prescribed SST and sea ice boundary conditions. Forcings in the radiation scheme follow Coupled Model Intercomparison Project Phase 5 (CMIP5) recommendations (Taylor et al. 2012) and include time-varying components of solar, greenhouse gas, ozone and aerosol forcing. For example, the impact of the major volcanic eruptions of Agung, El Chichón and Pinatubo on global surface air temperatures are well captured by the model ensemble (Hersbach et al. 2015). The simulations are run using the ECMWF integrated forecasting system (IFS) at T159 resolution (≈ 125 km) with 91 vertical levels. SST and sea ice boundary conditions were taken from the HadISST (v2.1) dataset. For each ensemble member, a unique SST realisation was drawn from the posterior probability distributions of the analysed fields. However, for the ENSO indices analysed here the difference in SST between the ensemble members is very small compared to the interannual variability (the Nino-3 indices from ERA-20CM are shown in Supplementary Figure 1). Geopotential height at 500 hPa is one of the few variables that is output with a daily temporal resolution from the ERA-20CM ensemble, so we will use this field to some measure of the storm track variability. Wintertime anomalies from the ERA-20CM ensemble were calculated relative to the ensemble mean climatologies but no detrending has been applied to any of the fields.

2.3 Signficance tests

The statistical significance of the correlation/regression differences between different periods in observations was calculated using a Monte Carlo bootstrap resampling method. In each of the periods, the two datasets were randomly resampled with replacement to produce dummy 31-year indices. The correlation/regression was then calculated for the two dummy datasets and the difference saved. This was performed 10,000 times to build up a distribution of the variability of the differences based on sampling uncertainty. Where the sign of the correlation/regression of full difference between the two periods is the same in at least 95% of the random samples, the difference is deemed significant at the 5% level. This method was used for the results shown in Figs. 3 and 5.

The significance of the difference between the median regression maps in Sect. 4 were calculated using the distributions of the 10,000 sampled ERA-20CM ensemble regression maps from each period. For each grid point, the sign of the median difference between the regression maps of the two periods was compared with the distribution of the 10,000 sampled ERA-20CM ensemble regression differences. Where the sign of the median difference between the two periods is the same in at least 95% of the sampled regression differences, the difference between the two periods is deemed significant at the 5% level. This method was used for the difference plots shown in Figs. 7, 8, 9, and 10.

The significance of the observed correlation and regression plots were calculated using a two-sided t-test. Care was taken to account for the effective number of degrees of freedom by accounting for the auto-correlation of the different datasets, following the method of Bretherton et al. (1999).

3 Wintertime North Pacific teleconnection in observations

We begin our analysis by assessing the ENSO teleconnection to the North Pacific in the observational datasets. Throughout this study we will use the standard Nino-3 region (90°W–150°W, 5°S–5°N, e.g. Trenberth 1997) as the index of ENSO. This is chosen over other ENSO SST indices (i.e. Nino 1 + 2, Nino-3.4 and Nino-4) because it exhibits the strongest relationship with extratropical North Pacific SLP anomalies over the full 1901–2010 analysis

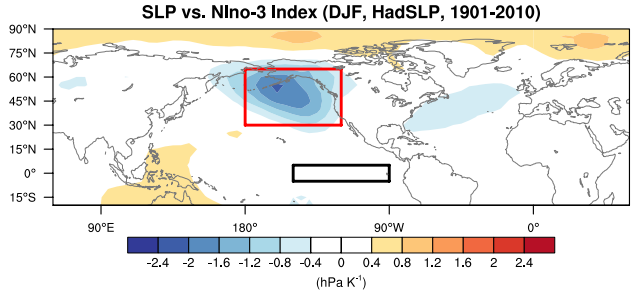

Fig. 1 Regression of the winter (DJF) SLP anomaly (from HadSLP) onto the Nino-3 SST anomaly index (mean index of the four SST datasets). The region for the North Pacific index is shown by the red box and the region for the Nino-3 index is shown by the black box

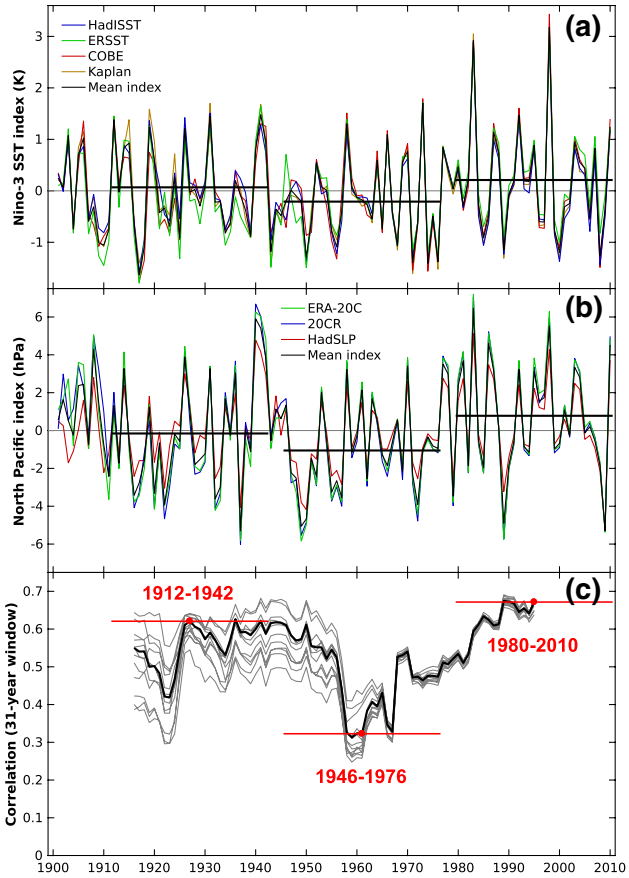

Fig. 2 **a** SST anomaly averaged over the Nino-3 region (90°W–150°W, 5°S–5°N) for four different SST datasets, as well as a mean index computed by averaging the four indices. **b** North Pacific indices, of negated North Pacific SLP anomalies averaged over the region shown in Fig. 1 (120°W–180°W, 30°N–65°N), for three different SLP datasets, as well as a mean index computed by averaging the three indices. **c** Correlation between the Nino-3 indices and North Pacific indices over moving 31-year windows. The grey lines shown the correlation between each different combination of Nino-3 and North Pacific indices (i.e. 4 (Nino-3) ×3 (North Pacific) = 12 combinations). The black line in **c** shows the correlation between the mean Nino-3 index and the mean North Pacific index. In **c**, red dots highlight 31-year periods when the indices are strongly correlated (1912–1942 and 1980–2010) and a period in the mid-century when the indices are weakly correlated (1946–1976). The horizontal black lines in **a** and **b** indicate the average values of the mean Nino-3 and North Pacific indices during these periods

period (Supplementary Figure 2). However, the results and conclusions throughout are qualitatively similar if the Nino-3.4 index is used.

Figure 1 shows the regression of the winter SLP anomaly (for HadSLP but the other datasets are similar) onto the mean Nino-3 index (which is an average of the Nino-3 indices from each of the SST datasets, Fig. 2). As found in numerous previous studies, ENSO exhibits a strong influence on the strength of the Aleutian Low, being deeper in El Nino years and weaker in La Nina years. The largest ENSO influence on the winter North Pacific is seen over the eastern part of the basin, outlined by the red box in Fig. 1 (120°W–180°W, 30°N–65°N). We will refer to the negated area-averaged SLP anomaly (i.e $-1 \times \mathrm{SLP}'$) in this region as the North Pacific index, although it is important to note that this region is located slightly further east than the commonly used North Pacific SLP index of Trenberth and Hurrell (1994) (c.f. 140°W–160°E, 30°N–65°N). Since the North Pacific index is negated, positive values indicate a strengthening of the Aleutian Low.

The Nino-3 indices for all of the SST datasets are shown in Fig. 2a, along with the North Pacific indices for all of the SLP datasets, shown in Fig. 2b. Also shown are the mean Nino-3 and mean North Pacific indices, computed by averaging across the indices from different datasets. The spread between both the Nino-3 and North Pacific indices is largest during the first half of the 20th century, when the raw observations were most sparse, indicative of the larger observational uncertainty. To analyse the variability of the link between ENSO and the North Pacific circulation, we calculated the correlation between the Nino-3 index and North Pacific index over moving 31-year windows. This calculation was performed for each individual pair of SST and SLP datasets and between the mean indices, time-series of the correlations are shown in Fig. 2c. For the mean indices, the link between the Nino-3 SSTs and North Pacific SLPs are strong over the most recent period and also in the early part of the 20th century, however, during the mid-century the relationship weakens substantially. Similar variability in the relationship between Nino-3 and the North Pacific is also seen in pairs of the individual SST and SLP datasets but in no pairing is the mid-century correlation similar to the late-century. There is little difference in the relationship between the Nino-3 index and North Pacific index for periods in the latter half of the 20th century but for periods before about 1970 there is substantial spread between the different pairs of individual datasets.

To further analyse the interdecadal variability we identify periods during which the ENSO teleconnection to the North Pacific is strong, in the early (1912–1942) and late (1980–2010) 20th century, and a mid-century period (1946–1976) during which the teleconnection was weaker (Fig. 2c). The difference in the interannual Nino-3-North Pacific index correlation between the mid-century period ($r = 0.32$) and the early/late-century periods ($r = 0.62/r = 0.67$) is substantial and is significant at the 5% level in both early and late periods (although the differences are slightly lower for correlations involving the ERSST Nino-3 index), as shown in Fig. 3. The correlation between the North Pacific index and SST anomalies in the early, mid and late-century periods are shown in Fig. 4. The correlation with North Pacific SSTs is similar in all periods, reflecting the forcing of the extratropical ocean by atmospheric circulation anomalies (e.g. Liu and Alexander 2007). The correlation with tropical Pacific SSTs, however, is very low during the mid-century, further highlighting the weak influence of tropical Pacific SSTs on the North Pacific circulation during this period.

In addition to analysing the influence of ENSO on the North Pacific index, we also performed similar analysis using the 1st empirical orthogonal function (EOF) of SLP over the North Pacific (following the method of, e.g., Yu and Kim 2011). The principal component timeseries of the 1st EOF of extratropical SLP is very similar to the North Pacific index, with a correlation coefficient of r = 0.94 over the 1901–2010 period. The patterns of variability associated with the 1st EOF are also similar in the early, mid and late-century periods, despite being calculated separately for each period (Supplementary Figure 3). The relationship between the 1st EOF of extratropical SLP and SST anomalies shows a similarly variable link with tropical Pacific SST anomalies, as seen in Fig. 4 for the North Pacific index. Therefore, the variable influence of the tropical Pacific SSTs on the North Pacific circulation in not sensitive to the method used to define the large-scale circulation anomalies.

To examine the teleconnection to the North Pacific in more detail we calculated regression maps of SLP anomalies against the mean Nino-3 index, which are shown for the early, mid and late-century periods in Fig. 5 (shown for HadSLP data, ERA-20C and 20CR yield similar results). The SLP anomaly regression in the North Pacific during the mid-century is weak compared to both the early period and the late period, when the teleconnection is strongest. The difference plots, also shown in Fig. 5, indicate the ENSO teleconnection to the Northeast Pacific is significantly stronger in both the early and late periods. The difference plots for the early and late periods contrast over the tropical East Pacific, where the difference is only significant in the late-century period (Fig. 5c) but this is not seen in ERA-20C and 20CR, so does not seem a robust result.

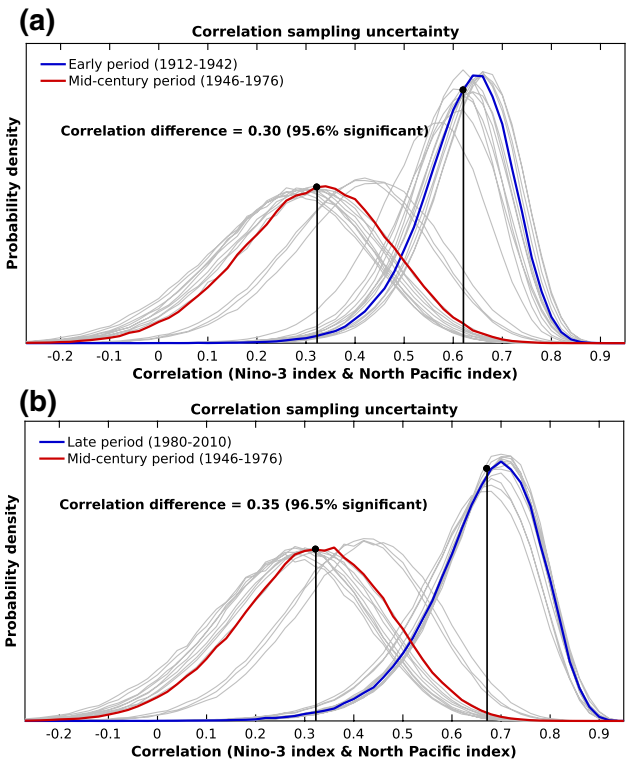

Fig. 3 Correlation sampling uncertainty, calculated using 10000 bootstrap resamples, comparing **a** 1912–1942 with 1946–1976, and **b** 1980–2010 with 1946–1976. The coloured lines show the distributions for the correlation between the mean Nino-3 and mean North Pacific indices; grey lines indicate distributions of the correlation between all the individual SST and SLP datasets

We also analysed cloud-cover anomalies regressed onto the Nino-3 index during these different periods (Supplementary Figure 4). In the late century period, there are large cloud cover anomalies over the central tropical Pacific, indicative of increased precipitation over this region during El Nino events. The cloud cover response to Nino-3 in the late-century period is stronger than in the mid-century period, although there is more missing data in this period. This suggests that the response of precipitation in the equatorial Pacific is larger in the late-century period than in the mid-century period. Unfortunately, there is very little cloud-cover data in the early-century period, so comparison with the mid-century period is not conclusive. To overcome these data issues, in the next section we will analyse the output of the ERA-20CM atmospheric model ensemble.

The average values of the Nino-3 and North Pacific indices over the early, mid and late-century periods are also shown in Fig. 2. The mid-century period (1946–1976) during which there is a weak relationship between Nino-3 SSTs and North Pacific circulation, is characterised by a weakening of the Aleutian Low and anomalously cool SSTs in the tropical Pacific. The late-century period, when the

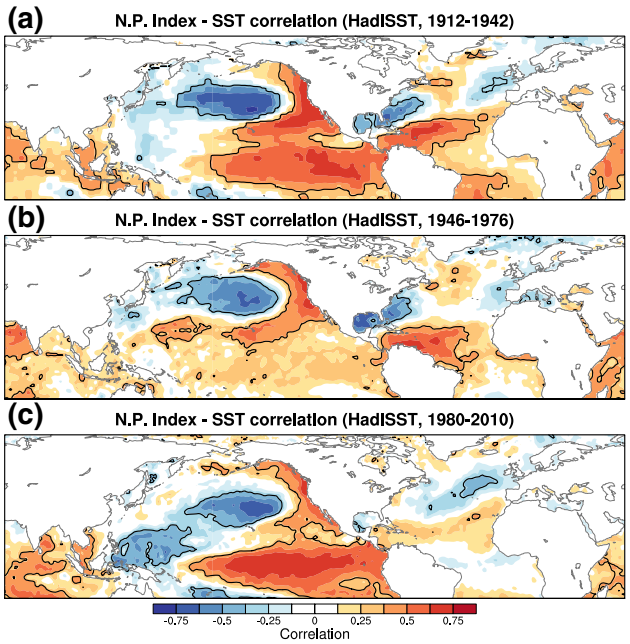

Fig. 4 Correlation of wintertime (DJF) SST anomalies (in HadISST) with the mean North Pacific index (i.e. black line in Fig. 2b) over the periods **a** 1912–1942, **b** 1946–1976, and **c** 1980–2010. The black contours indicate regions where the correlation is significant at the 5% level according to a two-sided t-test

relationship between Nino-3 SSTs and North Pacific circulation is strong, is characterised by a strengthening of the Aleutian Low circulation and anomalously warm tropical Pacific SSTs. These two periods correspond to those associated with interdecadal Pacific variability noted in previous studies (e.g. Trenberth and Hurrell 1994; Zhang et al. 1997; Deser et al. 2004) and the related Interdecadal Pacific Oscillation (e.g. Parker et al. 2007; Henley et al. 2015). However, the early-century period (1912–1942), during which the relationship between Nino-3 SSTs and North Pacific circulation is also strong, corresponds to fairly normal conditions in the Nino-3 and North Pacific indices. This suggests that the strong link between the tropical Pacific SSTs and the North Pacific circulation in the early and late-century periods might have be forced somewhat differently.

4 Wintertime North Pacific teleconnection in ERA-20CM

We now assess the interdecadal variability of the ENSO teleconnection to the North Pacific in the ERA-20CM atmospheric model ensemble. Comparing the observed variability with ERA-20CM allows us to test the extent to which the variability in the teleconnection is driven by SST variability, since the model is forced with observed SSTs at the lower boundary. Utilising the ten ensemble members in ERA-20CM we can investigate the role of internal variability due to atmospheric dynamics. Another advantage of using these simulations is that where the model has similar relationships between the SST and SLP fields, we can analyse other atmospheric variables such as precipitation or upper-level wind fields for which observational records over the entire 20th century do not exist.

The wintertime North Pacific index for each of the ERA-20CM members is shown in Fig. 6a. There is clear spread between the individual ensemble members but still an appreciable ensemble mean signal. To measure the strength of the ensemble mean signal relative to the ensemble spread we calculated the signal-to-noise ratio of the North Pacific index, defined here as the magnitude of the ensemble mean divided by the ensemble spread. The signal-to-noise ratio of the North Pacific index from ERA-20CM, along with the standard deviation of the Nino-3 SST index, over 31-year windows are plotted in Fig. 6b. The signal-to-noise ratio is largest in the late-century period (1980–2010) and is significantly lower during the mid-century period (1946–1976) during which the observed influence of the tropical Pacific on the North Pacific index is lower (i.e. Fig. 5). However, the signal-to-noise ratio is equally low in the early-century period (1912–1942) as the mid-century period. The low signal-to-noise in the early and mid-century periods corresponds to periods when the variability in the Nino-3 SST index was fairly weak, whereas in the late-century period the higher signal-to-noise ratio in the North Pacific index corresponds to a period of larger variability in the Nino-3 SST index. Also shown in Fig. 6b is the standard deviation of the Southern Oscillation Index[1] (SOI) over 31-year windows. The variability of the SOI closely follows that of the Nino-3 index, indicating that the weaker variability in the early and mid-century periods is not only seen in the tropical SST data but also the tropical SLP. The signal-to-noise in the North Pacific index, therefore, approximately follows the variability in the Nino-3 SSTs (and SLP anomalies associated with the SOI), such that when there are stronger anomalies in the tropical Pacific there tends to be a stronger ensemble mean signal in the North Pacific circulation. This suggests that the stronger link between the Nino-3 SSTs and North Pacific index in the late-century period may be due to larger magnitude tropical SST anomalies. However, this does not seem to be the case in the early-century period, when the Nino-3 SST (and SOI) variability is indistinguishable from the mid-century period.

[1] Downloaded from http://www.bom.gov.au/climate/current/soi2.shtml.

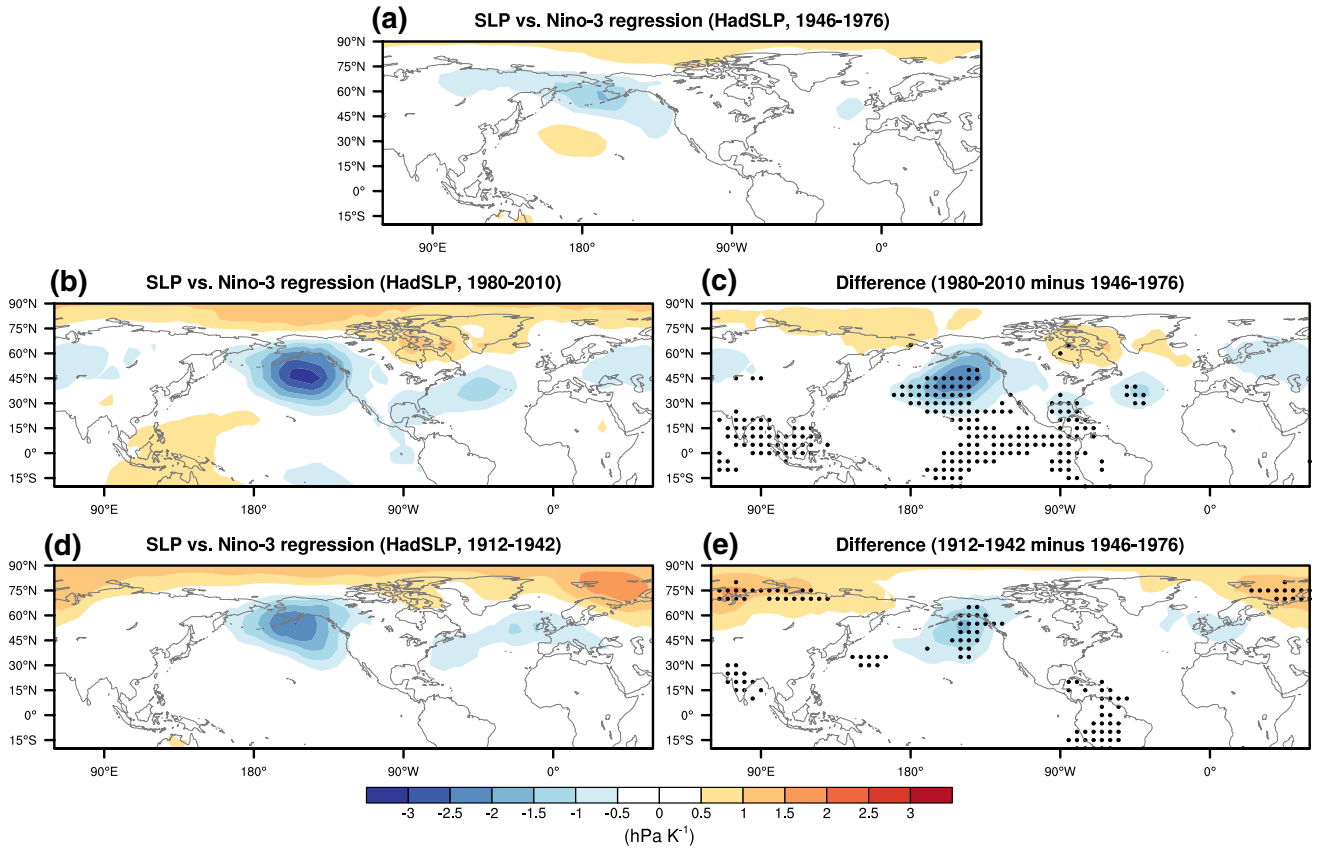

Fig. 5 SLP anomaly (from HadSLP) regressed onto the mean Nino-3 SST index over the periods **a** 1946–1976, **b** 1980–2010, and **d** 1912–1942. The difference between the regression over the mid-century period (1946–1976) and the recent (1980–2010) and early (1912–1942) periods are shown in **c** and **e**, respectively. Stippling in **c** and **e** indicates where the difference between the regressions over the two periods is significant at the 5% level, calculated using a bootstrap resampling over the two periods

4.1 Sampled ERA-20CM realisations

We next analyse how the ENSO teleconnection to the North Pacific is represented in the ERA-20CM simulations. Our aim here is to assess how the realisations of the North Pacific response to tropical SST variability correspond to observations. However, there are only ten ensemble members in ERA-20CM. To obtain a larger set of plausible ERA-20CM realisations we generate "sampled realisations", which are calculated by selecting one ensemble member from each year to produce a 110-year timeseries. Since the SST boundary condition of each ensemble member is very similar (i.e. Supplementary Figure 1), the North Pacific index from one year to the next are effectively indistinguishable between ensemble members. This was tested by calculating the autocorrelation of the North Pacific indices of each ensemble member with themselves and all other members, which are found to exhibit no appreciable difference (Supplementary Figure 4). The absence of year-to-year autocorrelation indicates that this is an acceptable resampling method, which would not be the case if there was significant autocorrelation in the ensemble members. Here, we compute 10,000 sampled realisations from the ERA-20CM ensemble and analyse the distribution of these equally plausible model realisations, which we can compare with the observations.

The distribution of the correlation between the Nino-3 and North Pacific index for the sampled ERA-20CM ensemble is shown in Fig. 6c. The median correlation of the sampled ERA-20CM ensemble is very similar to the observations during the late-century period, where the spread in the sampled ERA-20CM ensemble distribution is smaller than in earlier periods. The sampled ERA-20CM ensemble also well captures the weak correlation in the mid-century period, indicating that the North Pacific index was much less constrained by the SSTs in the mid century period than in the late-century period, when the tropical Pacific SST variability is larger (Fig. 6b). This is also evident in the increased spread of the correlation values during the mid-century period, suggesting that internal atmospheric variability is more important during this period compared with the late-century. In the early-century period, however, the median correlation of the sampled ERA-20CM ensemble

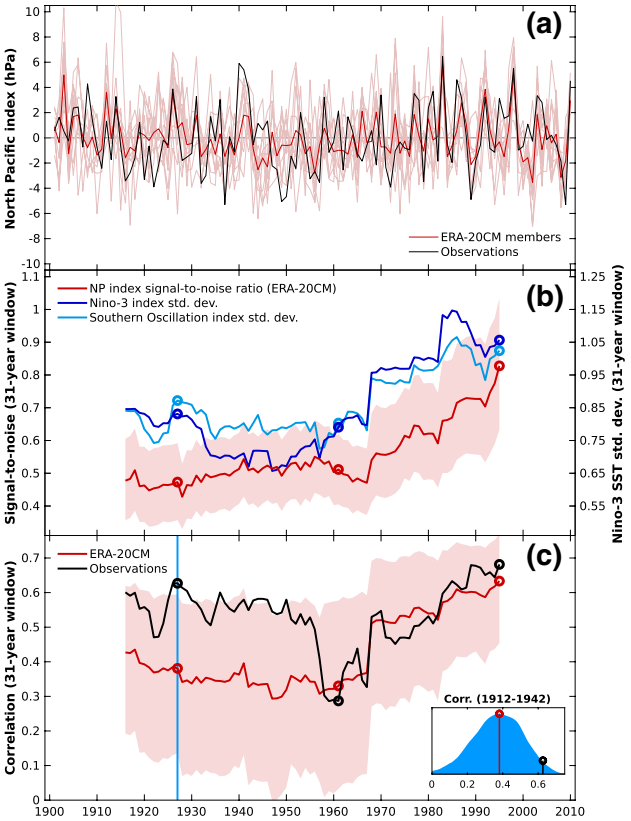

Fig. 6 **a** North Pacific indices in each of the 10 ERA-20CM ensemble members (in pink), the ERA-20C ensemble mean (in red), and the mean index from observations (in black, i.e. Fig. 2b). **b** Signal-to-noise ratio of the North Pacific indices in the ERA-20CM ensemble (shading indicates 5-95% sampling uncertainty from bootstrap resampling) along with the standard deviation of the Nino-3 index and the Southern Oscillation index, over moving 31-year windows. Prior to computing the standard deviation of the Southern Oscillation index the full index was scaled to match the standard deviation of the Nino-3 index, to allow for simpler comparison. **c** Distribution of the correlation of the sampled ERA-20CM North Pacific index realisations with the Nino-3 SST index, over 31-year windows. This was produced by randomly selecting one value of the North Pacific index from the ten ensemble members for each year, calculating the correlation with the Nino-3 index over 31-year windows, then repeating this process 10,000 times to yield a distribution of correlation values. The shading in **c** shows the 5–95% range of the distribution, the red line shows the median of the distribution and the black line shows the correlation from the observations (as in Fig. 2c). The circles in **b** and **c** highlight the values for the intervals 1912–1942, 1946–1976 and 1980–2010. The plot in the bottom right corner of **c** shows the distribution of correlation values from the randomly sampled ERA-20CM ensemble for the period 1912–1942, the median of the distribution is shown by the red circle and the observed correlation is shown by the black circle. The observed correlation lies within the top 2.7% of the randomly sampled correlation values during the period 1912–1942

is much lower than the correlation in observations. The full distribution of correlations reveals that 2.7% of the sampled ERA-20CM ensemble are as large as the observed correlation during the early period (i.e. Fig. 2c), which shows that such high correlations between the Nino-3 index and the North Pacific index are very unlikely occurrences in the simulations.

To further investigate the interdecadal modulation of the ENSO-North Pacific teleconnection in ERA-20CM, we now analyse maps of different atmospheric anomalies regressed onto the Nino-3 index. Figure 7 shows the median SLP regression maps of the sampled ERA-20CM ensemble in the early, mid and late-century periods, along with the differences between the adjacent periods. There is a stronger ENSO teleconnection to the North Pacific in the late-century compared to the mid-century, as in the observations. The teleconnection in the early-century period, however, is essentially the same as the mid-century period, similar to the previous correlation analysis, which further highlights the disparity between the observations and the simulations during the early-century.

Median precipitation regression maps of the sampled ERA-20CM ensemble are shown in Fig. 8. Compared with the mid-century period, in the late-century period there is significantly more precipitation over the central tropical Pacific per degree of the Nino-3 index. This indicates that the tropical Pacific SSTs exert a stronger influence in the late-century period when the variability in the Nino-3 SSTs is largest. This is consistent with previous studies that have emphasised the nonlinear response of tropical precipitation to SST anomalies, particularly during the El Nino phase (e.g. Hoerling et al. 1997, 2001). The nonlinearity arises due to the threshold dependence of convection in the tropics. Hoerling et al. 1997 showed that the nonlinear response of tropical precipitation alone can explain the nonlinearity in the extratropical circulation response to ENSO. The precipitation response in the sampled ERA-20CM ensemble is approximately twice as large in the late-century period as the mid-century period, which is proportional to the difference in the SLP response (i.e. Fig. 7). Since ERA-20CM closely matches the observations in the late and mid-century periods, this suggests that the difference in the strength of the ENSO-North Pacific teleconnection is largely due to the increase in Nino-3 SST variability in the late-century. In the early-century period, however, the precipitation anomalies in the sampled ERA-20CM ensemble are also largely indistinguishable from the mid-century period (Fig. 8e), similar to the SLP anomalies in the North Pacific (Fig. 7e).

To gain further insight into the extratropical atmospheric response to ENSO in the sampled ERA-20CM ensemble we also calculated regression maps for the zonal wind, u(250 hPa), and the storm track intensity, $s(Z_{500})$, shown in Figs. 9 and 10, respectively. Here $s(Z_{500})$ is the R.M.S. 2–8 day band-pass filtered geopotential height, at 500 hPa. In the late-century period there is a stonger southward displacement of the jet than in the mid-century period. This represents a strong equivalent barotropic response in the late-century, consistent with the deepening of the Aleutian Low

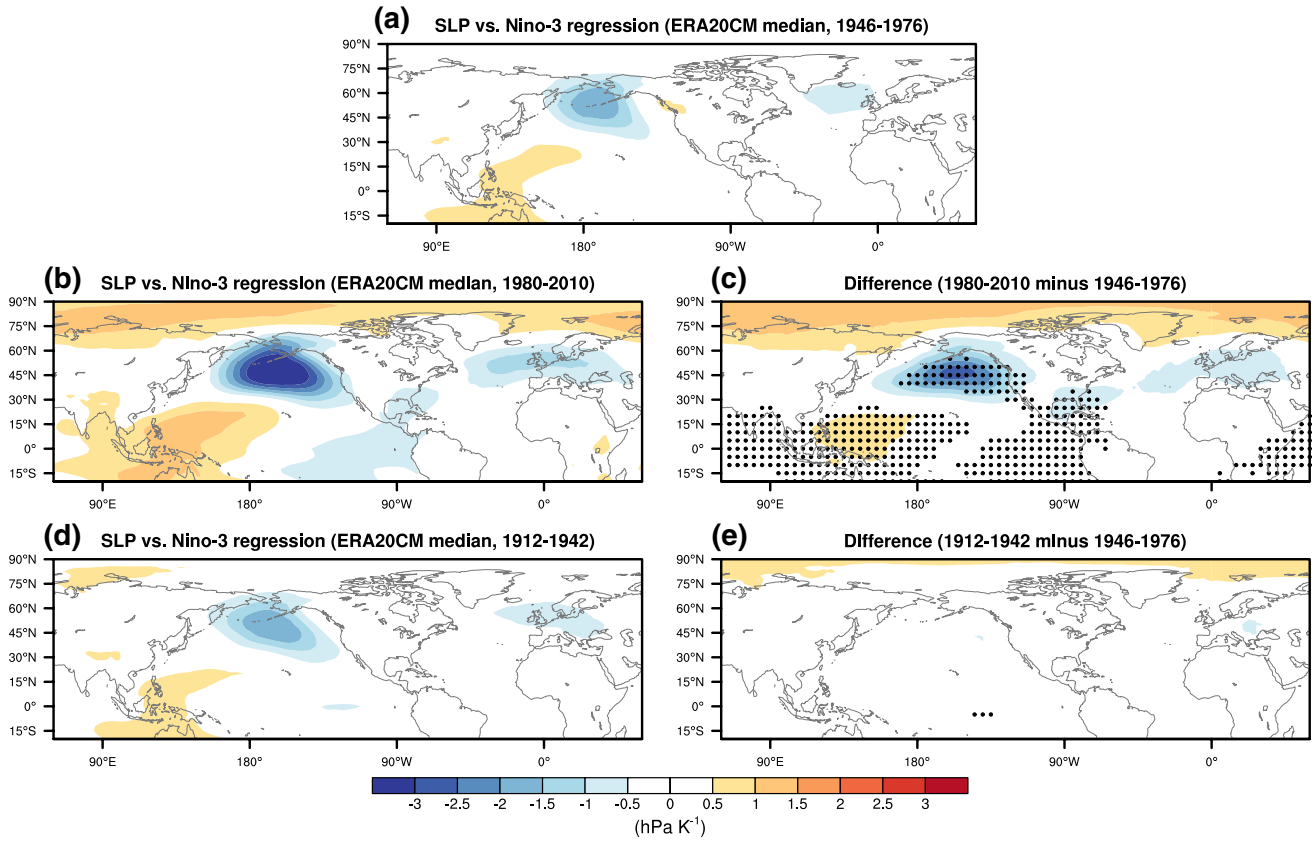

Fig. 7 SLP anomaly regressed onto the Nino-3 index for the sampled ERA-20CM realisations. The median of the distribution is shown for **a** 1946–1976, **b** 1980–2010, and **c** 1912–1942. The difference between the median regression over the mid-century period (1946–1976) and the recent (1980–2010) and early (1912–1942) periods are shown in **c** and **e**, respectively. Stippling in **c** and **e** indicates where the difference between the two periods is significant at the 5% level (see text for further details of the significance calculation)

seen in the SLP. The storm track also shows a southward displacement, which is aligned with the upper-level jet, albeit not as clearly significant. During the early-century period the ENSO connection to the upper-level jet and storm track are both indistinguishable from the mid-century period, as seen in both the precipitation and SLP anomalies.

4.2 Realisations of the 1912–1942 period

Overall, the model is able to clearly distinguish between the period of strong ENSO-North Pacific teleconnection in the late-century period and the weak teleconnection in the mid-century period. However, the strong link between ENSO and the North Pacific circulation in the early period is found to be a very unlikely occurrence in the model - exceeding the observed correlation only 2.7% of the realisations. In spite of this, it is useful to assess in what circumstances the model does have such a strong ENSO-North Pacific teleconnection. For example, is stronger tropical precipitation forcing required to give such a strong teleconnection? Or can the stronger correlation arise due to internal storm track variability in the extratropics? To investigate the strong teleconnection in the early-century we select a subset of the sampled ERA-20CM realisations that have a correlation between the Nino-3 index and the North Pacific index of between $r = 0.61$–0.63 in the early-century period, comparable with the observations (Fig. 6c). There are 201 of the 10,000 sampled ERA-20CM realisations that fall within this correlation range and these realisations are reasonably well distributed between ensemble members and years.[2]

The SLP and precipitation regression maps averaged over the high-correlation subset in the early-century period are shown in Fig. 11. By design, the SLP anomaly response to Nino-3 index closely matches the observed response in the early-century period (Fig. 11d). The high-correlation subset also has a stronger southward shift of the upper-level jet, u(250 hPa), consistent an equivalent barotropic strengthening of the Aleutian Low over the North Pacific (Fig. 12f).

[2] None of the ensemble members in any year makes up more than 40% of that years contribution to these 201 realisations. Excluding the realisations with the highest frequency ensemble member in any year had no noticable impact on the results.

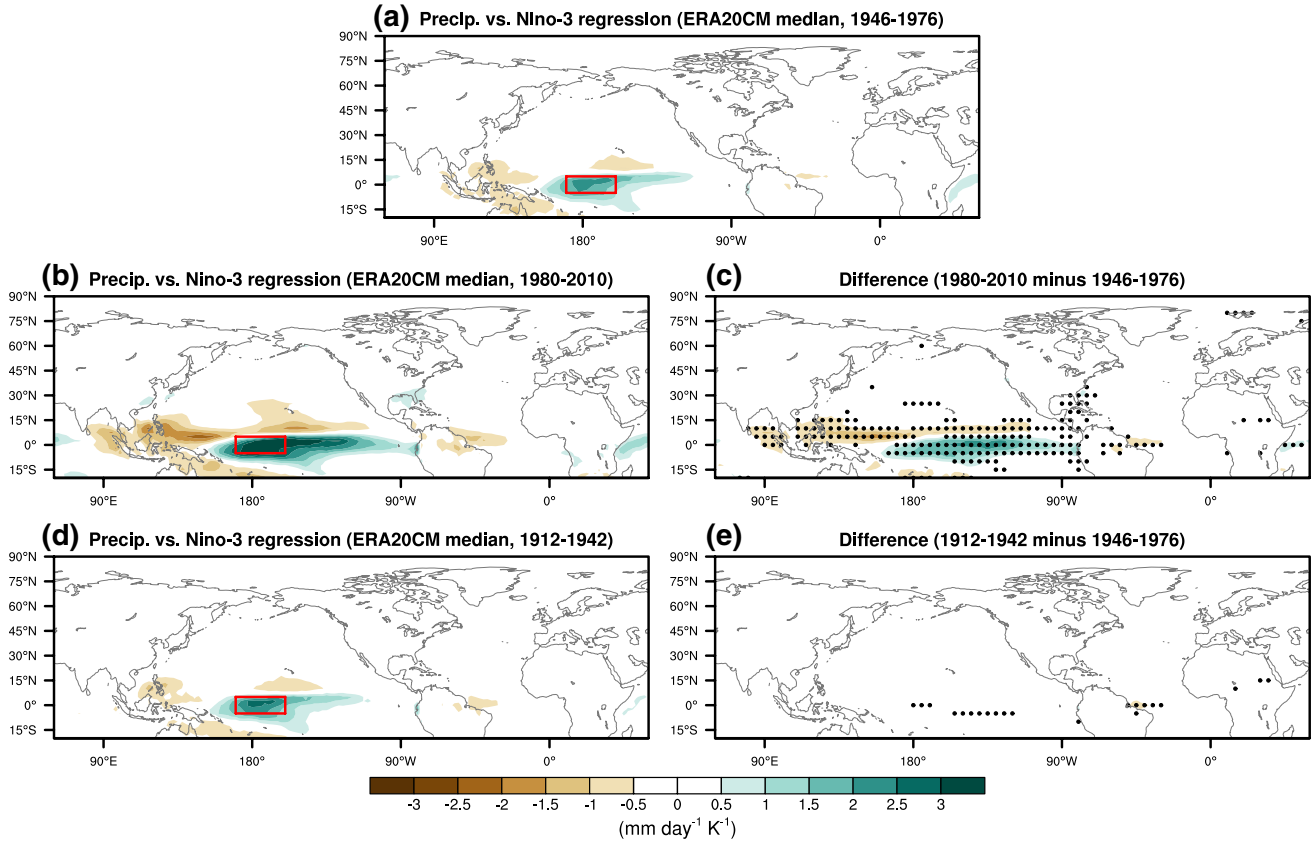

Fig. 8 Precipitation anomaly regressed onto the Nino-3 index for the sampled ERA-20CM realisations. The median of the distribution is shown for **a** 1946–1976, **b** 1980–2010, and **c** 1912–1942. The difference between the median regression over the mid-century period (1946–1976) and the recent (1980–2010) and early (1912–1942) periods are shown in **c** and **e**, respectively. Stippling in **c** and **e** indicates where the difference between the two periods is significant at the 5% level

This is accompanied by a distinct weakening of the storm track over the midlatitudes Northwest Pacific (Fig. 12e), corresponding to the stronger southward shift in the upper-level jet. More interestingly, however, the precipitation in the high-correlation subset in the early-century period is almost identical to the median of the full sampled ERA-20CM ensemble. This indicates that the stronger ENSO teleconnection to the North Pacific in the early-century period is not due to stronger tropical precipitation forcing in the equatorial Pacific, as is seen in the late-century period (i.e. Fig. 8b), but rather due to internal atmospheric variability in the extratropics. Distributions of the precipitation regressions over the central equatorial Pacific (shown by red boxes in Fig. 8) in the sampled ERA-20CM realisations are shown in Fig. 13. Almost none of sampled ERA-20CM realisations in the early-century period have a precipitation response that is stronger than even the lowest of the late-century realisations. This shows that the stronger North Pacific teleconnection in the model during the early-century period is never due to an increased tropical precipitation response to Nino-3 SSTs such as that seen in the late-century period.

The anomalously large storm track and upper-level jet responses in the high-correlation subset, therefore, suggest that the extratropical storm track variability, rather than tropical precipitation forcing, is acting in a way such that it strengthens the teleconnection in the early-century period. Whilst transient eddy fluxes typically act to reinforce the large-scale response to ENSO (e.g. Held et al. 1989; Seager et al. 2010), there is significant variability in the eddy forcing in the extratropics between different events, which creates a spread of possible extratropical circulation responses to similar forcing in the tropical Pacific (e.g. Hoerling and Ting 1994; Deser et al. 2017). The difference in the North Pacific SLP response to ENSO in the high-correlation subset compared with the full sampled ERA-20CM ensemble closely corresponds to a strengthening of the Aleutian Low in the North Pacific index region (Fig. 11).

To assess how the upper-level jet and storm track differences compare with a typical strengthening of the Aleutian Low, we have regressed these anomalies onto a normalised North Pacific index over the whole ERA-20CM dataset (Fig. 14). The differences between the upper-level jet and

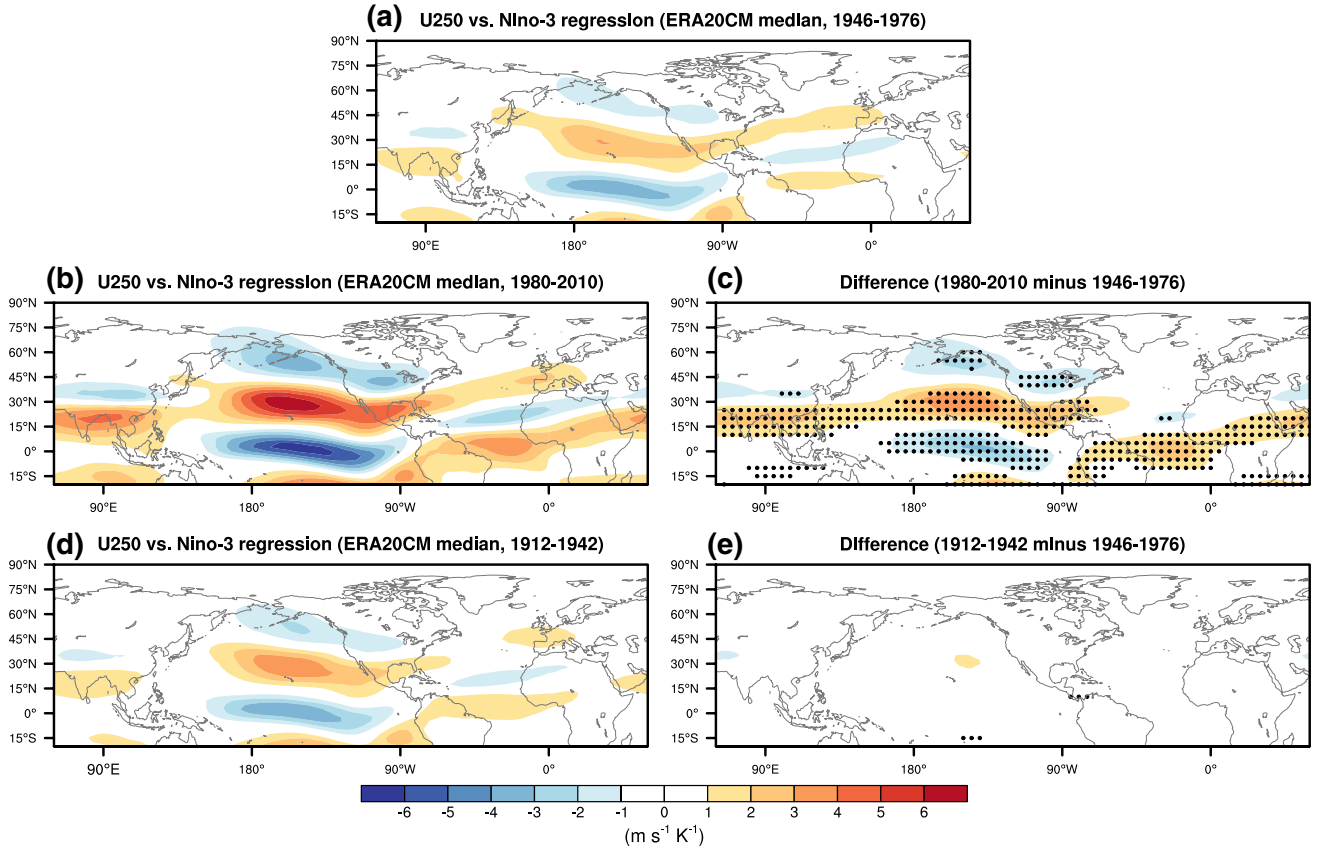

Fig. 9 u (250 hPa) anomaly regressed onto the Nino-3 index for the sampled ERA-20CM realisations. The median of the distribution is shown for **a** 1946–1976, **b** 1980–2010, and **c** 1912–1942. The difference between the median regression over the mid-century period (1946–1976) and the recent (1980–2010) and early (1912–1942) periods are shown in **c** and **e**, respectively. Stippling in **c** and **e** indicates where the difference between the two periods is significant at the 5% level

storm track response to ENSO in the high-correlation subset compared with the full sampled ERA-20CM ensemble are very similar to those associated with a strengthening of the North Pacific index. Since there are not velocity transients available in the ERA-20CM, it is not possible to directly estimate the contribution of transient eddies to the strengthening of the Aleutian Low. However, we can do similar analysis using the ERA-Interim reanalysis (1980–2016), since full atmospheric anomalies are provided at 6-h intervals. Maps of the anomalies regressed onto the normalised North Pacific index in ERA-Interim are also shown in Fig. 14. The SLP, upper-level jet and storm track anomalies are all very similar to those in ERA-20CM and therefore also similar to the differences seen between the high-correlation subset and the full sampled ERA-20CM ensemble.

Using the ERA-Interim reanalysis, however, we are able to calculate the zonal velocity tendency due to transient eddies. This gives a measure of the transient eddy forcing, $(du/dt)_{eddy}$, of the North Pacific index:

$$(du/dt)_{eddy} = \frac{\partial}{\partial y} S = -\frac{\partial}{\partial y} \nabla^{-2} (\nabla \cdot \overline{\mathbf{u}' \zeta'}), \quad (1)$$

where S is the streamfunction tendency due to 2–8 day band-pass filtered horizontal eddy vorticity fluxes at 250 hPa in the upper-troposphere[3] (following, e.g., Hoskins et al. 1983). The anomalous vorticity flux due to the transient eddies acts to force westerly anomalies in the eastern North Pacific basin (Fig. 14g), with the maximum in westerly eddy forcing occuring along the axis of the strong westerly anomalies (Fig. 14f). This suggests that the stronger Aleutian Low circulation in the high-correlation subset was likely forced by anomalously high transient eddy activity over the North Pacific, similar to that seen in the ERA-Interim data. The results from the ERA-20CM ensemble, therefore, suggest that anomalous storm track activity in the extratropical North Pacific could be responsible for the strong teleconnection from ENSO in the early-century period, rather than anomalously high forcing from tropical Pacific precipitation.

[3] The seasonal mean (DJF) tendencies are calculated for each year. These are then regressed onto the normalised North Pacific index.

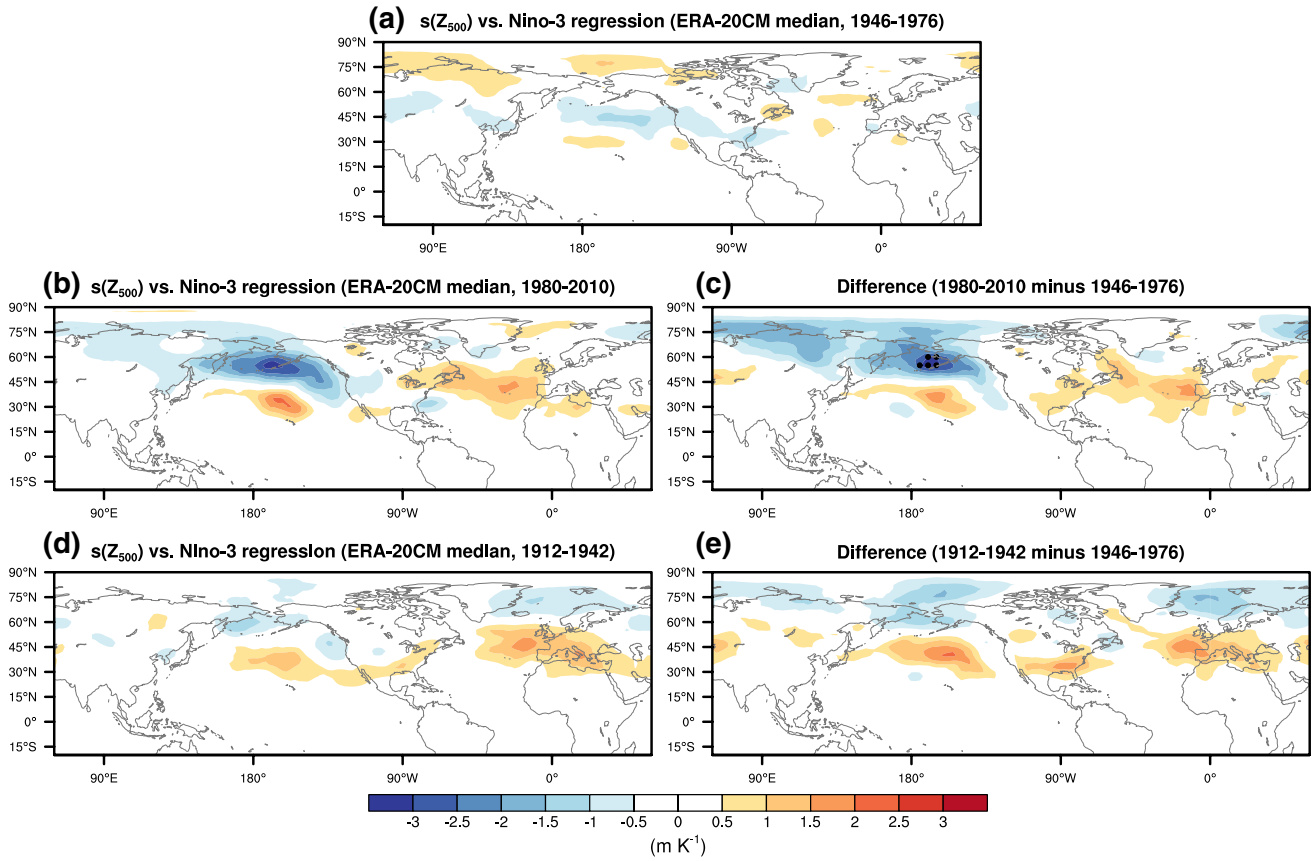

Fig. 10 $s(Z_{500})$ anomaly regressed onto the Nino-3 index for the sampled ERA-20CM realisations. The median of the distribution is shown for **a** 1946–1976, **b** 1980–2010, and **c** 1912–1942. The difference between the median regression over the mid-century period (1946–1976) and the recent (1980–2010) and early (1912–1942) periods are shown in **c** and **e**, respectively. Stippling in **c** and **e** indicates where the difference between the two periods is significant at the 5% level

5 Implications for extratropical North Pacific predictability

The weakness of the ENSO teleconnection to the North Pacific in the ERA-20CM ensemble during the early-century period has implications for assessing seasonal predictability. Taking the simulations at face value, in the early-century period anomalous internal atmospheric dynamics acted to amplify the observed strength of the ENSO teleconnection to the North Pacific. To consider the impact of this on seasonal predictability, we now assess the hindcast "skill" of the ERA-20CM ensemble. Whilst the ERA-20CM ensemble is clearly not directly comparable with initialised seasonal forecast systems, it may be a useful tool to test the amount of skill in the North Pacific circulation that can be derived from correct SSTs and to a lesser extent external forcing (i.e. in the absence of skill from initial conditions). Whilst this is an assumption, hindcasts of tropical SSTs typically exhibit high levels of skill in operational seasonal forecast systems (Weisheimer et al. 2009) and are the dominant source of skill for many regions (Smith et al. 2012).

To measure the "skill" of the ERA-20CM ensemble we calculate the correlation between the ERA-20CM ensemble mean and the observed North Pacific index, which is plotted in Fig. 15 for moving 31-year windows. The variability in correlation closely follows the variability in PNA skill demonstrated in seasonal hindcast experiments of the PNA by O'Reilly et al. (2017). In the mid-century period, the ensemble mean correlation disappears, owing to the weakness in the observed ENSO teleconnection to the North Pacific. However, in the early-century period the correlation is nearly as high as the late-century period, despite ERA-20CM only clearly being able to sufficiently simulate the teleconnection to the North Pacific in the late-century period (i.e. Fig. 6). In the early period, the model appears to be under-confident, which can be demonstrated by calculating the "ratio of predictable components" (RPC) following Eade et al. (2014)—shown in Fig. 15. This is a measure of the predictable signal in the ensemble compared with the correlation between the ensemble mean and observations. An RPC of 1 represents a model that properly captures the observed signal, whereas an RPC $>$ 1 indicates an under-confident ensemble. In the

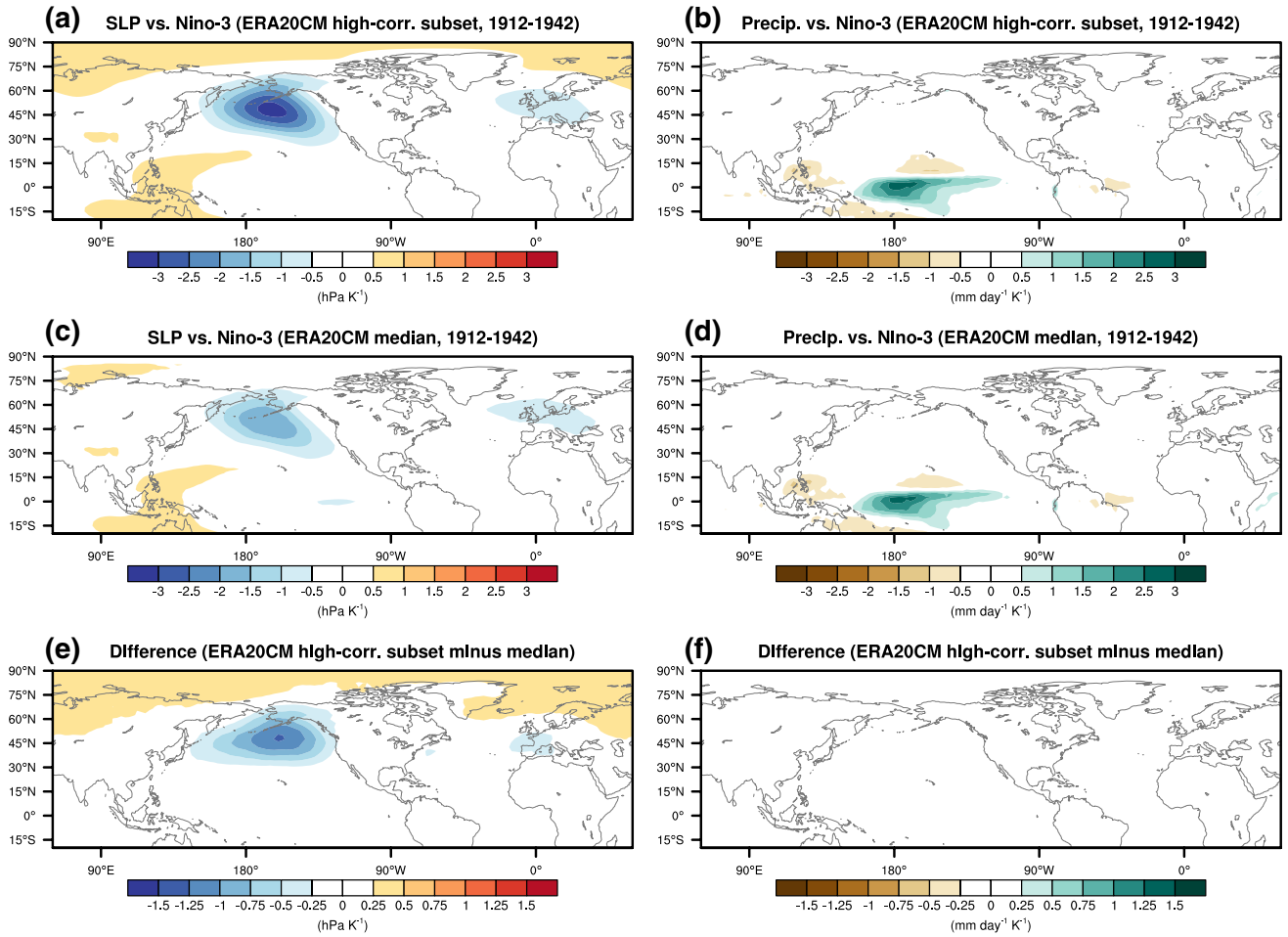

Fig. 11 Medians of the high-correlation subset (during 1912-1942) of the sampled ERA-20CM ensemble **a** SLP anomaly and **b** precipitation anomaly regressed onto the Nino-3 index. The median of the full sampled ERA-20CM ensemble **c** SLP anomaly and **d** precipitation anomaly regressed onto the Nino-3 index. The difference between the high-correlation subset and the median of the sampled ERA-20CM ensemble regressions for **e** SLP and **f** precipitation

early-century period, ERA-20CM is significantly under-confident, which suggests that the model is not capturing the predictable signal as strongly as would be expected based on the strong correlation with observations.

The under-confidence in the ERA-20CM ensemble could be related to a predictable pathway linking the tropical Pacific SSTs to the North Pacific circulation in observations that is weakly represented in the model. For example, this could be via interaction with the stratosphere. However, this would mean that this mechanism is only important for determining the strength of the teleconnection to the North Pacific during the early-century period and not during the mid and late-century periods, when the teleconnection is well captured by the ERA-20CM ensemble. It could, of course, be that SST observations are inaccurate during the early-century period and as a result the tropical forcing in the model is not strong enough to capture the observed teleconnection strength. The relative paucity of SST samples during the early-century period could be underestimating the magnitude of the seasonal SST anomalies in the equatorial Pacific. This could result in reduced magnitude tropical precipitation anomalies in the ERA-20CM simulations and the weaker teleconnection to the extratropical North Pacific. However, the variance in the Southern Oscillation Index in the early and mid-century period closely matches that seen in the Nino-3 SST indices, despite being calculated using surface pressure observations, indicating that perhaps the magnitude of SST anomalies in the early-century period are not being underestimated.

Another possibility is that the ERA-20CM is accurately representing the predictable pathways linking tropical Pacific SSTs and North Pacific circulation. If this is the case, the apparent under-confidence in ERA-20CM during the early-century period is due to internal extratropical atmospheric variability, which resulted in a fortuitously strong ENSO-North Pacific relationship and therefore a high correlation

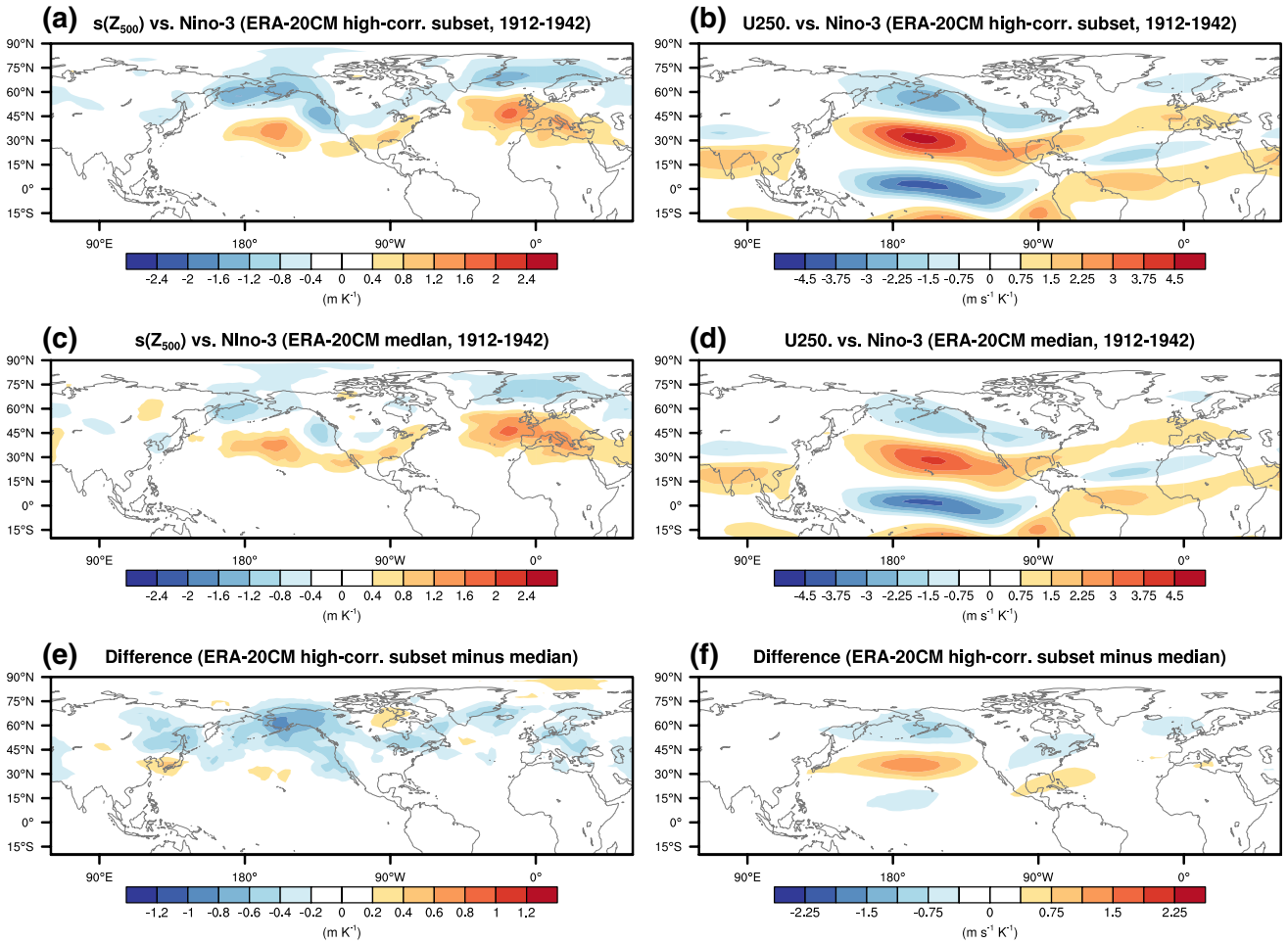

Fig. 12 Medians of the high-correlation subset (during 1912–1942) of the sampled ERA-20CM ensemble **a** $s(Z_{500})$ anomaly and **b** u(250 hPa) anomaly regressed onto the Nino-3 index. The median of the full sampled ERA-20CM ensemble **c** $s(Z_{500})$ anomaly and **d** u(250 hPa) anomaly regressed onto the Nino-3 index. The difference between the high-correlation subset and the median of the sampled ERA-20CM ensemble regressions for **e** $s(Z_{500})$ and **f** u(250 hPa)

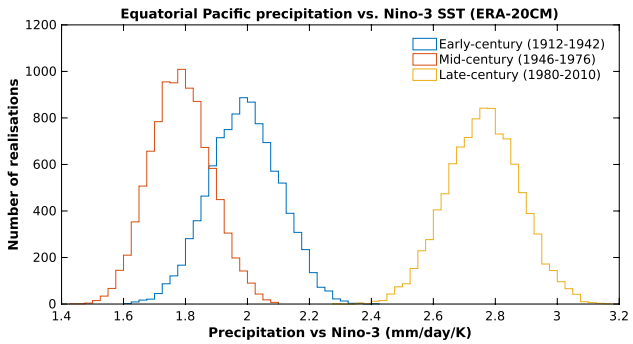

Fig. 13 Distributions of the equatorial Pacific precipitation regressed onto the Nino-3 timeseries in the 10,000 sampled ERA-20CM realisations for the early, mid and late-century periods

between the ensemble mean and observed North Pacific index. Based on the results presented here, it seems likely that internal extratropical variability played a significant role in the strong ENSO teleconnection to the North Pacific in the early-century, resulting in the apparent under-confidence in the ERA-20CM ensemble.

6 Summary

In this study we have analysed the interdecadal variability of the ENSO teleconnection to the wintertime extratropical North Pacific. Using a number of observation-based gridded datasets of SLP and SST we have shown that the teleconnection strength varies substantially from 1900 onwards. Specifically, 31-year periods in the early-century (1912–1942), mid-century (1946–1976) and the late-century (1980–2010) are identified when the ENSO teleconnection to the North

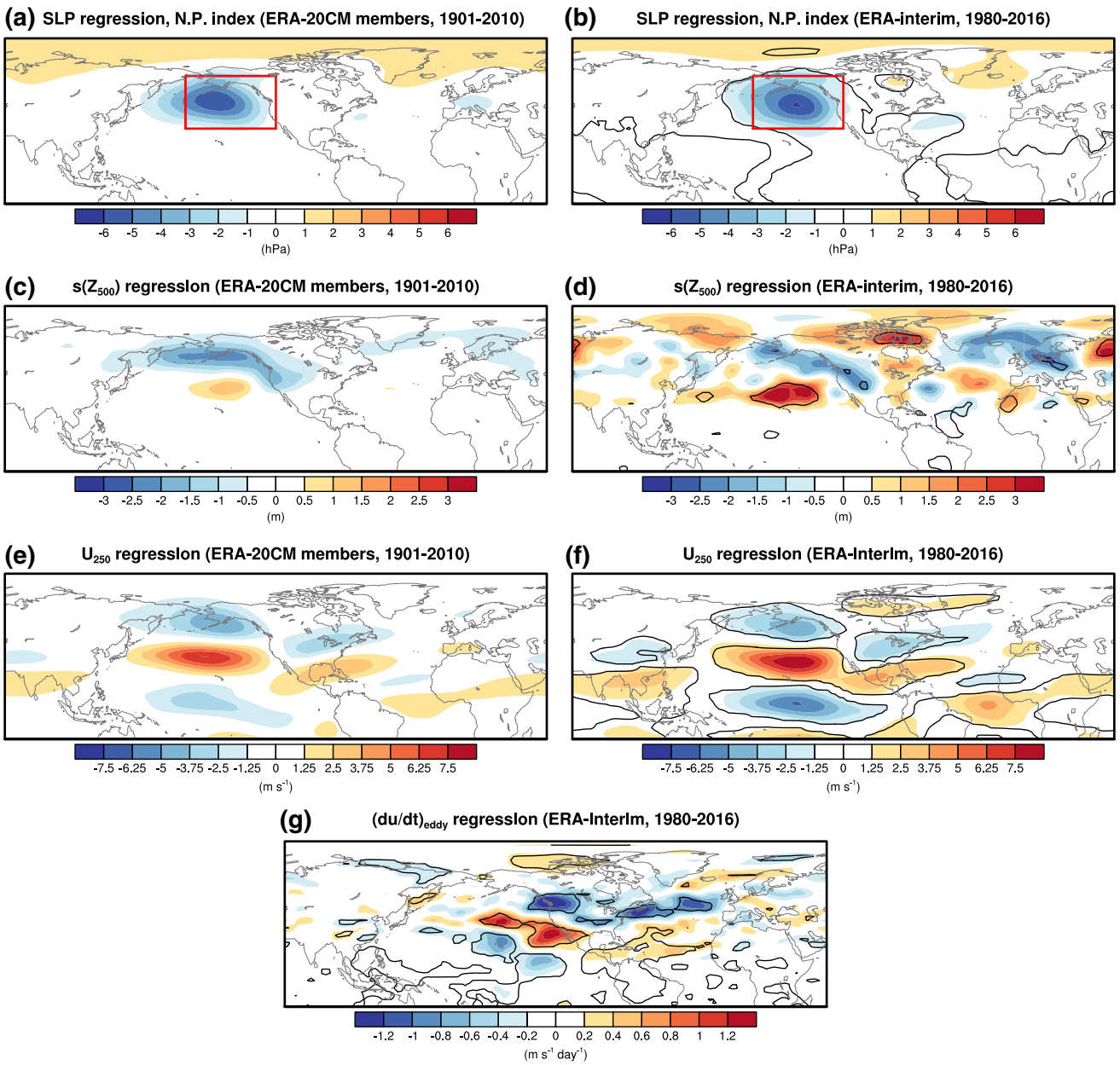

Fig. 14 Anomalies regressed onto the normalised North Pacific index in the ERA-20CM ensemble (over all 10 members, 1901–2010) and in the ERA-Interim reanalysis (1980–2016) for **a**, **b** SLP, **c**, **d** $s(Z_{500})$, and **e**, **f** u(250 hPa). **g** The regression of the anomalous transient eddy forcing, $(du/dt)_{eddy}$, at 250 hPa onto the normalised North Pacific index in the ERA-Interim reanalysis (1980–2016). The black contours indicate where the regression plots for the ERA-Interim data are significant at the 5% level, based on a a two-sided t-test. All shaded areas for the ERA-20CM regression maps exceed the 5% significance level, based on a two-sided t-test

Pacific circulation are found to be particularly strong, weak and strong respectively. In the early and late-century periods ENSO exhibits a similarly strong control on the SLP anomalies over the North Pacific, strongly increasing/decreasing the strength of the Aleutian Low in winters with positive/negative SST anomalies in the Nino-3 region. In the mid-century period, however, there is only a weak observed link between the Nino-3 SSTs and the North Pacific circulation. Since the variation is in the strength of interannual ENSO teleconnection, it most likely reflects some kind of dynamical natural climate variability (rather than forced by, e.g., greenhouse gases or aerosols), however, it is not clear from the observations alone what is responsible for the interdecadal variability. Many of the more useful observational fields are not available in the early and mid-century periods (e.g. upper atmospheric winds, precipitation over oceans), so to investigate further we analysed the ERA-20CM ensemble of atmospheric model simulations between 1900 and 2010.

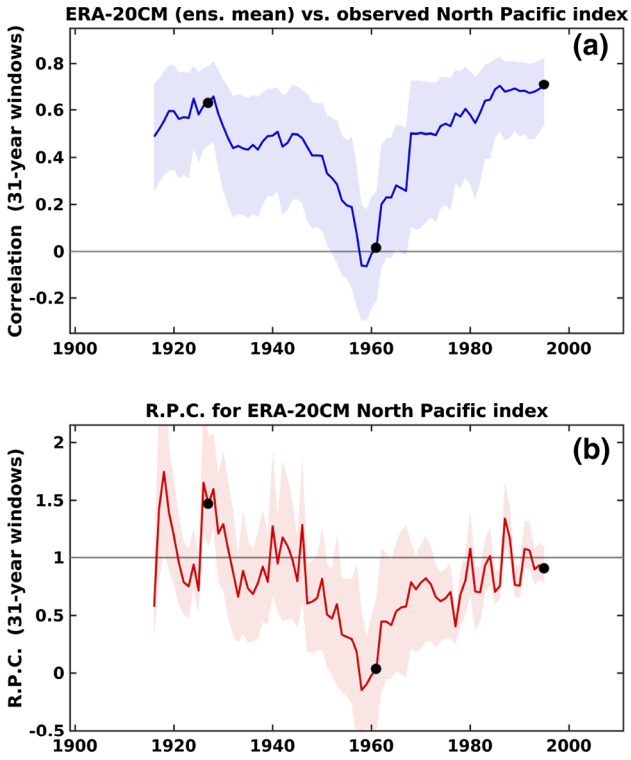

Fig. 15 **a** Correlation between the ERA-20CM ensemble mean North Pacific index and observed North Pacific index over moving 31-year windows. **b** Ratio of predictable components for the ERA-20CM North Pacific index. The black dots highlight the values for the early, mid and late-century periods discussed in the text. Shading indicates the 5–95% confidence interval based on a bootstrap with replacement method, performed 10,000 times

The ENSO teleconnection to the North Pacific in the sampled ERA-20CM ensemble is weak in the mid-century period and is substantially stronger in the late-century, closely following the variability in the observed teleconnection (i.e. Fig. 6c). In the late century period, the stronger teleconnection to the North Pacific is accompanied with an approximately proportional increase in equatorial Pacific precipitation response to Nino-3 SSTs. The increased tropical precipitation response is associated with a increased variability in the observed Nino-3 SSTs in the late-century period and series of strong extreme El Nino events (i.e. Nino-3 anomaly $> +1$ K), which have a nonlinear influence on tropical precipitation anomalies (e.g. Hoerling et al. 1997). This is consistent with the increased cloud-cover response in the late-century period seen in the observations (i.e. Supplementary Figure 4). In the early-century, however, the sampled ERA-20CM also exhibits a weak teleconnection to the North Pacific, which is in contrast to the strong teleconnection seen in observations. In fact the response of the model to Nino-3 SSTs in the early-century periods is almost indistinguishable to the mid-century period in terms of North Pacific SLP, upper-level jet and storm track responses and in terms of tropical Pacific precipitation anomalies. The strong ENSO teleconnection to the North Pacific seen in observations during the early-century period is a highly unlikely occurrence in the ERA-20CM model, with only 2.7% of the sampled ERA-20CM realisations exceeding the observed ENSO-North Pacific index correlation (i.e. Fig. 6c).

In the subset of ERA-20CM realisations that exhibit similar strength to the observed ENSO-North Pacific teleconnection during the early-century period, there are large differences in extratropical circulation but not in tropical precipitation anomalies (i.e Fig. 11). This suggests that the high correlation in the early century period is largely due to internal extratropical variability, rather than being forced by a larger precipitation response to ENSO over the equatorial Pacific, as in the late-century period. This conclusion is supported by the study of Deser et al. (2017), in which they demonstrated that internal variability can generate a wide range of responses to similar ENSO events. In the ERA-Interim dataset, an intensification of the North Pacific index is associated with anomalous eddy vorticity fluxes that force the zonal jet anomalies (i.e. Fig. 14g). Comparing this with the ERA-20CM simulations suggests that the early-century period in observations was likely associated with anomalous storm track activity, which resulted in the strong teleconnection to the North Pacific seen in the observations.

The varying nature of the ENSO teleconnection to the North Pacific has implications for seasonal forecasting. During the mid-century period, when there is a weak teleconnection to the North Pacific, seasonal hindcast skill is reduced over both the Pacific and Euro-Atlantic sectors (O'Reilly et al. 2017). However, during the early and late-century periods, the strong observed ENSO teleconnection to the North Pacific is largely associated with increased hindcast skill. The analysis presented here suggests that strong forcing from precipitation anomalies in the equatorial Pacific is responsible for the increased skill in the late-century period, which is well captured in the ERA-20CM ensemble. The high levels of skill in the early-century period are associated with a signal that is too weak in the ensemble, indicating that hindcasts may be considered under confident during this period. The ERA-20CM suggests that extratropical internal atmospheric variability played an important role in strengthening the ENSO teleconnection to the North Pacific, therefore the high levels of skill in hindcasts of this period may be considered to have arisen due to a somewhat fortuitously strong ENSO-North Pacific relationship.

Acknowledgements Discussions with Tim Woollings were invaluable during this study. Comments from Shoshiro Minobe, Laure Zanna and Tim Woollings proved hugely helpful to improve the manuscript. COR was funded by Natural Environment Research Council Grant number NE/M005887/1.

References

Allan R, Ansell T (2006) A new globally complete monthly historical gridded mean sea level pressure dataset (HadSLP2): 1850–2004. J Clim 19(22):5816–5842

Bjerknes J (1969) Atmospheric teleconnections from the equatorial Pacific. Mon Weather Rev 97(3):163–172

Branstator G (1985) Analysis of general circulation model sea-surface temperature anomaly simulations using a linear model. Part I: Forced solutions. J Atmos Sci 42(21):2225–2241

Bretherton CS, Widmann M, Dymnikov VP, Wallace JM, Bladé I (1999) The effective number of spatial degrees of freedom of a time-varying field. J Clim 12(7):1990–2009

Cayan DR, Redmond KT, Riddle LG (1999) Enso and hydrologic extremes in the western united states. J Clim 12(9):2881–2893

Compo GP, Whitaker JS, Sardeshmukh PD (2006) Feasibility of a 100-year reanalysis using only surface pressure data. Bull Am Meteorol Soc 87(2):175–190

Compo GP, Whitaker JS, Sardeshmukh PD, Matsui N, Allan RJ, Yin X, Gleason BE, Vose RS, Rutledge G, Bessemoulin P et al (2011) The twentieth century reanalysis project. Q J R Meteorol Soc 137(654):1–28

Dee D, Uppala S, Simmons A, Berrisford P, Poli P, Kobayashi S, Andrae U, Balmaseda M, Balsamo G, Bauer P et al (2011) The ERA-Interim reanalysis: configuration and performance of the data assimilation system. Q J R Meteorol Soc 137(656):553–597

Deser C, Alexander MA, Xie S-P, Phillips AS (2010) Sea surface temperature variability: patterns and mechanisms. Annu Rev Mar Sci 2:115–143

Deser C, Phillips AS (2006) Simulation of the 1976/77 climate transition over the North Pacific: sensitivity to tropical forcing. J Clim 19(23):6170–6180

Deser C, Phillips AS, Hurrell JW (2004) Pacific interdecadal climate variability: linkages between the tropics and the North Pacific during boreal winter since 1900. J Clim 17(16):3109–3124

Deser C, Simpson IR, McKinnon KA, Phillips AS (2017) The Northern Hemisphere extra-tropical atmospheric circulation response to ENSO: how well do we know it and how do we evaluate models accordingly? J Clim

Diaz HF, Hoerling MP, Eischeid JK (2001) ENSO variability, teleconnections and climate change. Int J Climatol 21(15):1845–1862

Dunstone N, Smith D, Scaife A, Hermanson L, Eade R, Robinson N, Andrews M, Knight J (2016) Skilful predictions of the winter North Atlantic Oscillation one year ahead. Nat Geosci 9(11):809–814

Eade R, Smith D, Scaife A, Wallace E, Dunstone N, Hermanson L, Robinson N (2014) Do seasonal-to-decadal climate predictions underestimate the predictability of the real world? Geophys Res Lett 41(15):5620–5628

Gershunov A, Barnett TP (1998a) ENSO influence on intraseasonal extreme rainfall and temperature frequencies in the contiguous United States: observations and model results. J Clim 11(7):1575–1586

Gershunov A, Barnett TP (1998b) Interdecadal modulation of ENSO teleconnections. Bull Am Meteorol Soc 79(12):2715–2725

Held IM, Lyons SW, Nigam S (1989) Transients and the extratropical response to El Niño. J Atmos Sci 46(1):163–174

Henley BJ, Gergis J, Karoly DJ, Power S, Kennedy J, Folland CK (2015) A tripole index for the interdecadal pacific oscillation. Clim Dyn 45(11–12):3077–3090

Hersbach H, Peubey C, Simmons A, Berrisford P, Poli P, Dee D (2015) ERA-20CM: a twentieth-century atmospheric model ensemble. Q J R Meteorol Soc 141(691):2350–2375

Hirahara S, Ishii M, Fukuda Y (2014) Centennial-scale sea surface temperature analysis and its uncertainty. J Clim 27(1):57–75

Hoerling MP, Kumar A, Xu T (2001) Robustness of the nonlinear climate response to ENSOs extreme phases. J Clim 14(6):1277–1293

Hoerling MP, Kumar A, Zhong M (1997) El Niño, La Niña, and the nonlinearity of their teleconnections. J Clim 10(8):1769–1786

Hoerling MP, Ting M (1994) Organization of extratropical transients during El Nino. J Clim 7(5):745–766

Horel JD, Wallace JM (1981) Planetary-scale atmospheric phenomena associated with the Southern Oscillation. Mon Weather Rev 109(4):813–829

Hoskins BJ, James IN, White GH (1983) The shape, propagation and mean-flow interaction of large-scale weather systems. J Atmos Sci 40(7):1595–1612

Huang B, Banzon VF, Freeman E, Lawrimore J, Liu W, Peterson TC, Smith TM, Thorne PW, Woodruff SD, Zhang H-M (2015) Extended reconstructed sea surface temperature version 4 (ERSST. v4). Part I: upgrades and intercomparisons. J Clim 28(3):911–930

Kaplan A, Cane MA, Kushnir Y, Clement AC, Blumenthal MB, Rajagopalan B (1998) Analyses of global sea surface temperature 1856–1991. J Geophys Res Oceans 103(C9):18567–18589

Kent EC, Kennedy JJ, Smith TM, Hirahara S, Huang B, Kaplan A, Fukuda Y et al. (2017) A call for new approaches to quantifying biases in observations of sea surface temperature. Bull Am Meteorol Soc 98(8):1601–1616

Liu Z, Alexander M (2007) Atmospheric bridge, oceanic tunnel, and global climatic teleconnections. Rev Geophys 45:RG2005

Mantua NJ, Hare SR, Zhang Y, Wallace JM, Francis RC (1997) A Pacific interdecadal climate oscillation with impacts on salmon production. Bull Am Meteorol Soc 78(6):1069–1079

McCabe GJ, Dettinger MD (1999) Decadal variations in the strength of ENSO teleconnections with precipitation in the western United States. Int J Climatol 19(13):1399–1410

McPhaden MJ, Zebiak SE, Glantz MH (2006) ENSO as an integrating concept in earth science. Science 314(5806):1740–1745

Minobe S (1997) A 50–70 year climatic oscillation over the North Pacific and North America. Geophys Res Lett 24(6):683–686

Minobe S, Mantua N (1999) Interdecadal modulation of interannual atmospheric and oceanic variability over the North Pacific. Prog Oceanogr 43(2):163–192

Namias J (1976) Some statistical and synoptic characteristics associated with El Niño. J Phys Oceanogr 6(2):130–138

O'Reilly CH, Heatley J, MacLeod D, Weisheimer A, Palmer TN, Schaller N, Woollings T (2017) Variability in seasonal forecast skill of Northern Hemisphere winters over the twentieth century. Geophys Res Lett 44:5729–5738

Parker D, Folland C, Scaife A, Knight J, Colman A, Baines P, Dong B (2007) Decadal to multidecadal variability and the climate change background. J Geophys Res 112:D18115

Poli P, Hersbach H, Dee DP, Berrisford P, Simmons AJ, Vitart F, Laloyaux P, Tan DG, Peubey C, Thépaut J-N et al (2016) ERA-20C: an atmospheric reanalysis of the twentieth century. J Clim 29(11):4083–4097

Rayner N, Parker DE, Horton E, Folland C, Alexander L, Rowell D, Kent E, Kaplan A (2003), Global analyses of sea surface temperature, sea ice, and night marine air temperature since the late nineteenth century. J Geophys Res 108(D14): 4407. https://doi.org/10.1029/2002JD002670

Ropelewski CF, Halpert MS (1987) Global and regional scale precipitation patterns associated with the El Niño/Southern Oscillation. Mon Weather Rev 115(8):1606–1626

Sarachik ES, Cane MA (2010) The El Nino-Southern oscillation phenomenon. Cambridge University Press, Cambridge

Sardeshmukh PD, Hoskins BJ (1988) The generation of global rotational flow by steady idealized tropical divergence. J Atmos Sci 45(7):1228–1251

Scaife A, Arribas A, Blockley E, Brookshaw A, Clark R, Dunstone N, Eade R, Fereday D, Folland C, Gordon M et al (2014) Skillful long-range prediction of European and North American winters. Geophys Res Lett 41(7):2514–2519

Seager R, Naik N, Ting M, Cane M, Harnik N, Kushnir Y (2010) Adjustment of the atmospheric circulation to tropical Pacific SST anomalies: variability of transient eddy propagation in the Pacific-North America sector. Q J R Meteorol Soc 136(647):277–296

Smith DM, Scaife AA, Kirtman BP (2012) What is the current state of scientific knowledge with regard to seasonal and decadal forecasting? Environ Res Lett 7(1):015602

Taylor KE, Stouffer RJ, Meehl GA (2012) An overview of CMIP5 and the experiment design. Bull Am Meteorol Soc 93(4):485–498

Trenberth KE (1997) The definition of El Niño. Bull Am Meteorol Soc 78(12):2771–2777

Trenberth KE, Branstator GW, Karoly D, Kumar A, Lau N-C, Ropelewski C (1998) Progress during TOGA in understanding and modeling global teleconnections associated with tropical sea surface temperatures. J Geophy Res Oceans 103(C7):14291–14324

Trenberth KE, Hurrell JW (1994) Decadal atmosphere-ocean variations in the Pacific. Clim Dyn 9(6):303–319

Trenberth KE, Shea DJ (1987) On the evolution of the Southern Oscillation. Mon Weather Rev 115(12):3078–3096

Wallace JM, Gutzler DS (1981) Teleconnections in the geopotential height field during the Northern Hemisphere winter. Mon Weather Rev 109(4):784–812

Wang B (1995) Interdecadal changes in El Nino onset in the last four decades. J Clim 8(2):267–285

Weisheimer A, Doblas-Reyes F, Palmer T, Alessandri A, Arribas A, Déqué M, Keenlyside N, MacVean M, Navarra A, Rogel P (2009) ENSEMBLES: A new multi-model ensemble for seasonal-to-annual predictionsSkill and progress beyond DEMETER in forecasting tropical Pacific SSTs. Geophys Res Lett 36(21)

Weisheimer A, Schaller N, O'Reilly C, MacLeod DA, Palmer T (2017) Atmospheric seasonal forecasts of the twentieth century: multi-decadal variability in predictive skill of the winter North Atlantic Oscillation (NAO) and their potential value for extreme event attribution. Q J R Meteorol Soc 143(703):917–926

Woodruff SD, Worley SJ, Lubker SJ, Ji Z, Eric Freeman J, Berry DI, Brohan P, Kent EC, Reynolds RW, Smith SR et al (2011) ICOADS Release 2.5: extensions and enhancements to the surface marine meteorological archive. Int J Climatol 31(7):951–967

Wu A, Hsieh WW (2003) Nonlinear interdecadal changes of the El Niño-Southern oscillation. Clim Dyn 21(7):719–730

Yu J-Y, Kim ST (2011) Relationships between extratropical sea level pressure variations and the central Pacific and eastern Pacific types of ENSO. J Clim 24(3):708–720

Zhang Y, Wallace JM, Battisti DS (1997) ENSO-like interdecadal variability: 1900–93. J Clim 10(5):1004–1020